# Electrochemical Nitrogen Reduction Reaction Performance of Single-Boron Catalysts Tuned by MXene Substrates

Shisheng Zheng,[#] Shunning Li,[#] Zongwei Mei, Zongxiang Hu, Mihai Chu, Jiahua Liu, Xin Chen, and Feng Pan*

School of Advanced Materials, Peking University, Shenzhen Graduate School, Shenzhen 518055, People's Republic of China

S *Supporting Information*

ABSTRACT: A boron (B) center, which has an electronic structure mimicking the filled and empty d orbitals in transition metals, can effectively activate the triple bond in N_2 so as to catalyze the nitrogen reduction reaction (NRR). Here, by means of density functional theory, we have systematically investigated the catalytic performance of a single B atom decorated on two-dimensional transition metal carbides (MXenes). The B-doped Mo_2CO_2 and W_2CO_2 MXenes exhibit outstanding catalytic activity and selectivity with limiting potentials of −0.20 and −0.24 V, respectively. Importantly, we have found that, although a high tendency of B-to-adsorbate electron donation can promote the hydrogenation of $*N_2$ to $*N_2H$, it would also severely hamper the $*NH_2$ to $*NH_3$ conversion due to the strong B−N bonding. Such an electron-donation effect can be reasonably tuned by the transition metal in the MXene substrate, which enables us to achieve optimized catalytic performance with a certain moderate degree of electron donation.
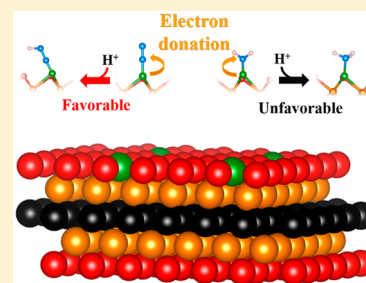
As a basic component for the production of fertilizers that sustain the global food supply, ammonia (NH_3) is one of the most important chemicals in modern life.[1] Consequently, its synthesis has attracted intense interest all over the world for decades.[2−4] The current industrial manufacture of NH_3 relies on the energy-intensive Haber−Bosch process, which requires harsh reaction conditions (∼500 °C and ∼30 MPa) and involves coactivation of the reactant hydrogen (H_2) and nitrogen (N_2) gases with the use of heterogeneous iron-based catalysts.[5] Though exothermic (46.1 kJ/mol) in nature,[6] NH_3 synthesis at ambient conditions is extremely challenging because of the strong N≡N triple bond (dissociation energy: 945 kJ/mol)[7] and the large HOMO−LUMO gap (10.82 eV).[8] Nevertheless, taking its inspiration from N_2 biological fixation with nitrogenase enzymes in bacteria,[4,9,10] the electrochemical N_2 reduction reaction (NRR) to NH_3 holds great promise to provide a green and sustainable way for NH_3 production at room temperature and atmospheric pressure.[11−14] To the present day, a variety of catalysts based on transition metals[15−20] and their oxides,[21−26] nitrides,[27−30] and carbides[31,32] have been proposed for electrochemical NRR. Unfortunately, an efficient heterogeneous catalyst that can exhibit sufficiently low overpotential, high Faradaic efficiency, and long durability is still beyond reach.[13,14] Developing inexpensive, selective, and stable catalysts for electrochemical NRR therefore remains one of the fundamental issues in this field.

From a mechanistic point of view, NRR through electrochemical approaches proceeds through a series of N_2H_x and NH_x intermediates, among which the formation of N_2H, i.e., the inclusion of the first $H^+/e^−$ pair to the N_2 molecule, is generally the rate-determining step.[13] In this context, the

weakening of the N≡N bond upon the adsorption of a N_2 molecule on the catalyst surfaces is of paramount importance. For transition metal catalysts, the N_2 would denote electrons from its bonding orbitals to the unoccupied d orbitals of the transition metal while accepting electrons from the occupied d orbitals to the antibonding π^*-orbitals of N_2.[33] This electron back-donation promotes N_2 activation for the successive reactions. Recently, it was demonstrated that strong back-donation from boron (B) centers to N_2 can effectively realize N_2 reduction.[34,35] Following up on this finding, several studies have shown that a single B atom decorated on graphene, g-C_3N_4, black phosphorus, et al. can lead to relatively high reactivity for N_2 reduction.[36−40] However, for most of the above catalysts, the substrates are composed of main group elements, whereas the effect of d orbitals of transition-metal-containing substrates on the catalytic activity of B centers has not yet been explored. The investigation of the change in catalytic performance, tuned by the interplay between transition-metal d orbitals and B p orbitals, could contribute to a greater chance for finding suitable catalysts for NRR and understanding the roles of the B centers.

Herein, we investigate the potential of two-dimensional transition-metal carbides ($M_{n+1}C_n$), so-called MXenes, as the substrates for single-boron catalysts. In the formula, "M" represents early transition metals (Ti, Zr, Hf, V, Nb, Ta, Cr, Mo, and W), and n = 1, 2, or 3. Owing to their high electronic conductivity, large surface areas, and tunable surface composition,[41,42] MXenes are receiving increasing interest as

promising candidates for use in catalysis.[31,32,43−48] It is worth mentioning that the basal planes of MXenes are generally terminated by functional groups (−OH, −F, and −O) after hydrogen fluoride treatment during their synthesis.[49] Recent studies have also shown that high-temperature annealing can transform the OH-terminated MXene surfaces into O terminations.[50] Therefore, in this work, we have chosen the O-terminated M_2CO_2 MXenes as representatives for the investigation of single-boron NRR catalysts. State-of-the-art density functional theory (DFT) calculations[37,51−54] with dispersion corrections (calculation details can be found in the Supporting Information) are carried out to unravel the mechanism of NRR for single-boron catalysts and to find out the potential MXene substrates that exhibit high catalytic activity and desirable catalytic selectivity. From our calculations, we propose that B-doped Mo_2CO_2 and W_2CO_2 are ideal candidates for electrochemical NRR and that a certain moderate degree of B-center-mediated electron donation, as controlled by the transition-metal d orbitals in the substrate, is required for the superior catalytic performance. This study highlights the tenability of single-boron catalysis via d-band substrates and can shed light on the design of novel electrochemical NRR catalysts based on B centers.

Previous studies have found that the coverage of surface groups on MXenes is far from uniform, which can therefore introduce an appreciable amount of oxygen vacancies for the O-terminated MXenes.[50,55] It can be anticipated that the introduced B atom would prefer to place itself at the O-vacancy site, taking the form of a substitutional B dopant in the O layer (Figure 1a). We have examined the intrinsic stability of a single B atom in MXenes by calculating the binding energies between B and MXenes with O vacancies (Table S1). Our calculation results of over 2 eV indicate sufficiently strong binding of the B atom to the MXenes, which is further
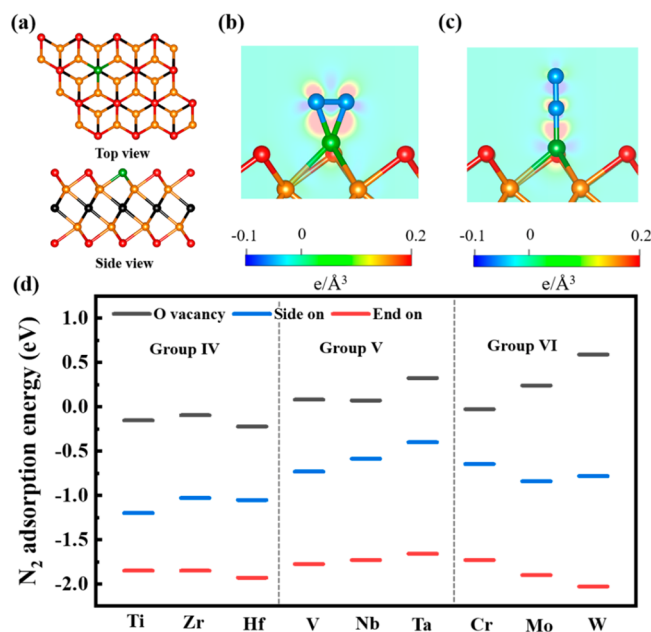
confirmed by the relatively high barrier for B diffusion out of the O vacancy and the kinetic stability of the B-doped MXene exhibited in the ab initio molecular dynamics simulations (Figure S1). Therefore, the B atoms on MXenes will show little tendency to aggregate into clusters,[56] which guarantees good durability of the B-doped MXene catalysts during operation.

As mentioned above, electron back-donation can exert significant influence on NRR performance. Here, we find that for all of the single-boron MXene catalysts, the N_2 gas can be preferentially chemisorbed on the B center. Two kinds of adsorption patterns (side-on and end-on) are examined, both of which involve a substantial charge redistribution with characteristics of strong electron back-donation effects, as demonstrated by the charge density difference shown in Figure 1b,c (exemplified by B-doped Mo_2CO_2). Charge accumulates between B and N atoms, indicating the formation of B−N bonds, which can be accounted for by the N_2 to B electron donation.[34,35] The electrons on the B atom are back-donated to the antibonding π^* orbitals of N_2, thus reducing the N−N bond strength and resulting in the charge depletion region between two N atoms. The N−N bond length is also elongated from 1.11 to 1.21 and 1.14 Å for side-on and end-on adsorption, respectively, with 0.6 and 0.4 e excess electrons accumulated on N_2.

Comparing between the adsorption of N_2 on a B center and that on an O vacancy (Figure 1d), it is found that N_2 adsorption is energetically favored on a B center for both patterns, while adsorption on an O vacancy involves a more positive adsorption energy for each MXene catalyst. This indicates that the interaction between N_2 and O vacancies on MXenes is much weaker than that between N_2 and B, demonstrating the role of B centers for serving as catalytic active sites for NRR. N_2 adsorption via the end-on pattern is considerably more stable than that via the side-on pattern, which is also observed in other systems.[37,52] Therefore, the side-on pattern is not eligible for the following investigation of NRR on B-doped MXenes.

From the end-on adsorption of N_2, two typical pathways, i.e., the distal and alternating pathways wherein the protons consecutively attack the N atoms, are illustrated in Figure 2a.[4,11,14] In the distal pathway, the remote N atom is hydrogenated first, releasing the first NH_3 molecule, after which protons add to the remaining N atom to produce the second NH_3. In the alternating pathway, both N atoms are hydrogenated simultaneously, and only when the fifth proton is added to the N_2 can the first NH_3 be released. Occasionally, NRR can proceed by a mixed pathway that shifts between distal and alternating pathways (there are three mixed pathways available).[4,31,57] To evaluate the NRR performance, all of the elementary steps associated with distal and alternating pathways (Figure S4) are taken into consideration, and the reaction pathway for each B-doped MXene is determined by the most energetically favorable intermediate at each hydrogenation step. Our DFT-D3 results predict that NRR on all of these catalysts prefers to adopt the mixed pathway with the following intermediates: $*N_2 \rightarrow *N\text{-}NH \rightarrow *N\text{-}NH_2 \rightarrow *NH\text{-}NH_2 \rightarrow *NH \rightarrow *NH_2 \rightarrow *NH_3$ (Mixed 3 pathway), which is different from classical materials.[11] Intriguingly, for group IV (Ti, Zr, Hf) and V (V, Nb, Ta) MXenes, the last hydrogenation step is identified as the potential limiting step (PDS), similar to that of B-doped graphene.[36] This is unlike most of the transition-metal-based catalysts,[58,59] as well as group VI (Cr, Mo, W) MXenes in our

Figure 1. (a) Top and side views of the structure of B-doped MXene. Charge density difference of N_2 adsorption on B-doped Mo_2CO_2 via (b) side-on and (c) end-on patterns. Color code: metal in orange, carbon in black, oxygen in red, boron in green, and nitrogen in blue. (d) Adsorption energies of N_2 on O vacancies and B centers for different MXenes.
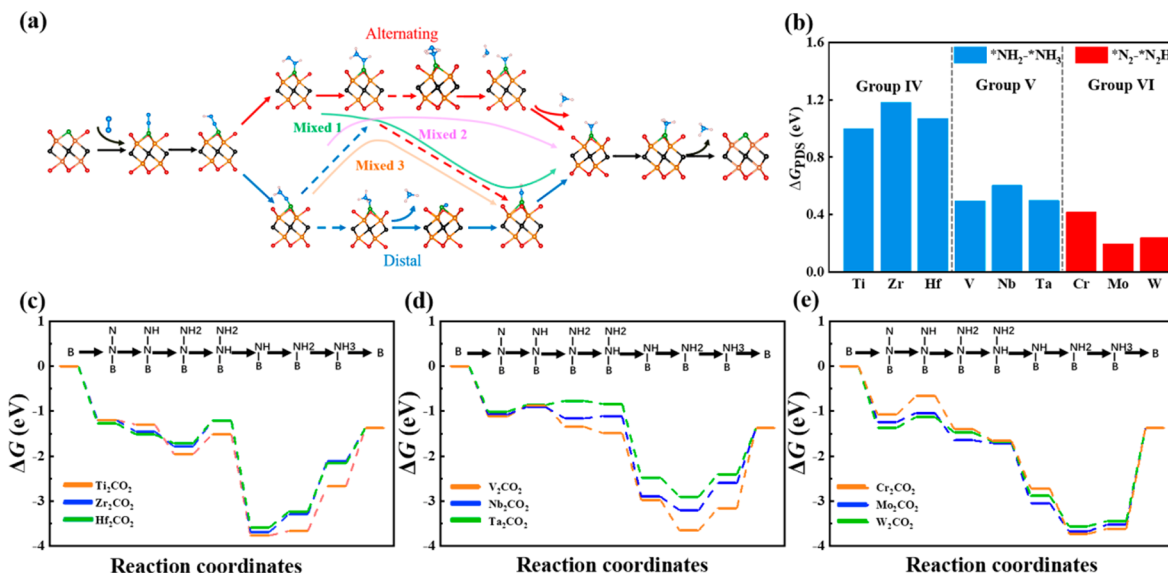
Figure 2. (a) Schematic illustration of the distal, alternating, and mixed pathways for electrochemical NRR. (b) Free energy change at PDS for all single-boron MXene catalysts. The PDS for group IV and V MXenes is $*NH_2 \rightarrow *NH_3$, while for group VI MXenes, the PDS is $*N_2 \rightarrow *N\text{-}NH$. The free energy profiles for NRR catalyzed by group (c) IV, (d) V, and (e) VI MXenes with B centers.
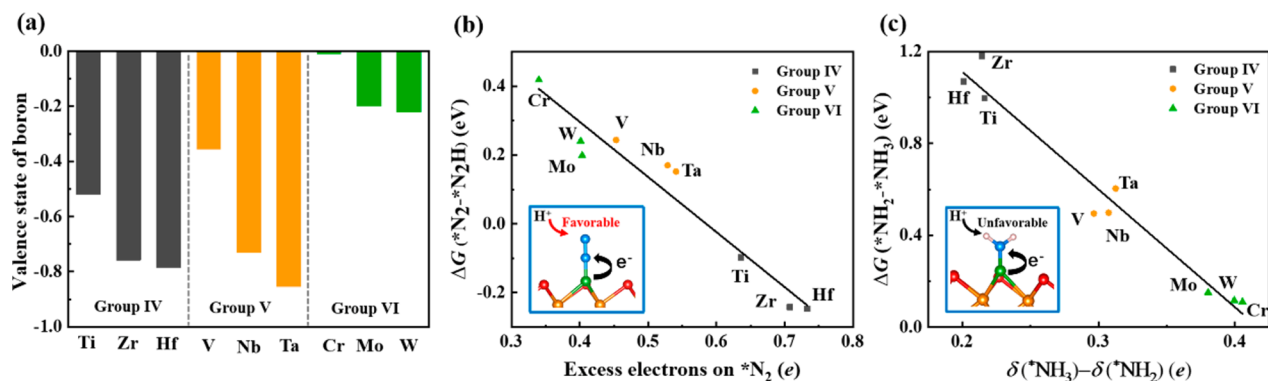

Figure 3. (a) Valence states of the B atom in B-doped MXenes. (b) Free energy change of the first hydrogenation step as a function of the excess electrons on N_2 when it is adsorbed on the B center. (c) Free energy change of the last hydrogenation step as a function of the change in the total electrons (δ) between $*NH_3$ and $*NH_2$ adsorbates.

study, for which the PDS is imposed by the first hydrogenation step.

Figure 2b summarizes the free energy change at the PDS for all B-doped MXenes, in which a downward trend can be discerned from group IV to group VI. For group V and VI MXenes, the Gibbs free energy change for the PDS (ΔG_{PDS}) is well below that on the Ru(0001) surface (1.08 eV), indicating favorable intrinsic catalytic activity for NRR. Among them, the B-doped Mo_2CO_2 and W_2CO_2 exhibit the most promising catalytic activity, with ΔG_{PDS} as low as 0.20 and 0.24 eV, respectively. These values are competitive with other theoretically studied single-boron NRR catalysts, such as B-doped g-C_3N_4 (0.20 eV),[37] MoS_2 (0.35 eV),[39] and graphene (0.41 eV).[36]

The Gibbs free energy profiles corresponding to the B–N_xH_y intermediates are depicted in Figure 2c−e. It is apparent that the profiles for MXenes with transition metal elements in the same group in the periodic table show remarkable similarity, which is to be expected due to their similar electronic properties.[60] For group IV MXenes, the first hydrogenation step is exothermic, while for other MXenes an energy input is required. Meanwhile, from group IV to group

VI, the $*NH_2 \rightarrow *NH_3$ step is becoming more thermodynamically accessible to proceed, with ΔG decreasing from more than 1.0 eV to around 0.1 eV. In addition, we discovered that the release of the second NH_3 from the catalyst surface generally requires a rather large activation energy, making the desorption of the formed NH_3 the rate-determining step. Nevertheless, the $*NH_3$ species could be easily attacked by protons to form NH_4^+ in strongly acidic solutions,[32,61−63] rendering the desorption process to proceed without any obstacle in the catalytic cycle.

In order to further understand the superior catalytic activity of the B-doped Mo_2CO_2 and W_2CO_2 for electrochemical NRR, we inspect the valence state of the B atom along the reaction pathway for all MXene catalysts through Bader charge analysis. As can be seen in Figure 3a, the B atom is accommodated as anions in the substrate, with the injection of electrons from the transition metal to the B p orbitals. Hence, the B center acts as an electron transmitter, while the substrate acts as an electron reservoir for the regulation of charge in the catalytic cycle (Figure S5). The interplay between transition-metal d orbitals and B p orbitals can effectively control the valence state on the B atom, as well as
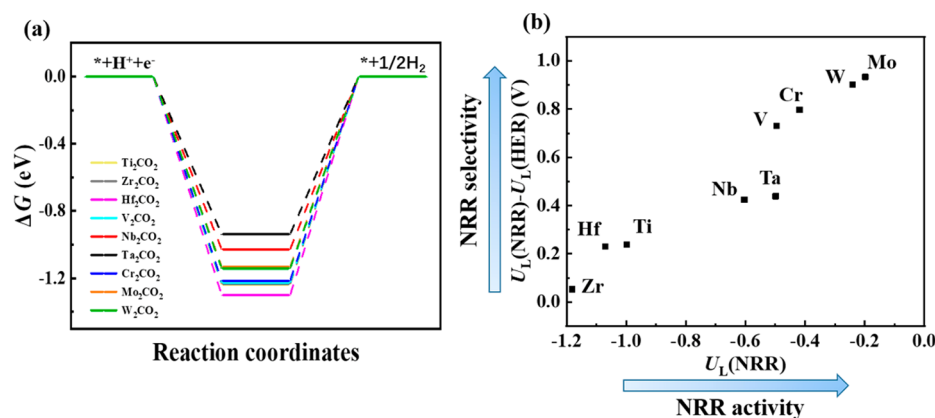
Figure 4. (a) Catalytic activity for HER. (b) Plots of $U_L(NRR) - U_L(HER)$ vs $U_L(NRR)$ illustrating the NRR performance of single-boron catalysts with MXene substrates.

the charge variation along the pathway. The smaller amount of accumulated charge on B in group VI MXenes would imply that the B center may have a lower tendency to inject electrons to the adsorbates.[39] This is further substantiated by the fact that there is a lower amount of excess electrons on N_2 for group VI MXenes according to Bader charge analysis. The partial density of states in Figure S7 also reveals the occupation of N π^* orbitals. These occupied states (in the range of $-2-0$ eV below the Fermi level) overlap with the B p states, demonstrating the electron back-donation from B to N_2. We can see that the degree of electron donation, quantified by the excess electron on N_2, is linearly correlated with the energy input for the addition of a hydrogen atom (Figure 3b). B-doped Cr_2CO_2, with electron deficiency on B, is reluctant to donate electrons and thus displays the highest uphill free energy at the first hydrogenation step. It is worth mentioning that the B atom in group IV and VI MXenes is ferromagnetic, while it is not in group V MXenes (Figures S6 and S7). The occurrence of spin-polarization means that these electrons are unpaired and have higher energy than the non-spin-polarized electrons in the same system.[53,64] Hence, spin-polarized electrons on B are more prone to pair with foreign electrons, which can be the reason behind the higher degree of electron back-donation for group IV MXenes as compared with those for group V, even though the valence states of B for both are on the same scale.

The high tendency of electron donation compels us to treat the B center in group IV MXenes as a comparatively strong Lewis base. This, however, can be detrimental to the last hydrogenation step, as shown in Figure 3c. The strong bonding between the B center and $*NH_2$ intermediate, arising from such electron transfer, would lead to an approaching eight-electron configuration of the $*NH_2$ species. This corresponds to a relatively small difference in total electrons between $*NH_3$ and $*NH_2$ (~0.2 e for group IV MXenes) and a substantially large energy penalty for the final H^+/e^- gain on $*NH_2$ due to its stable electronic structure. In contrast, if the B−N bonding is weak, the $*NH_2$ species would be far from the noble-gas-like eight-electron configuration, in which case, this N atom has a radical character and therefore will be more energetically favored to be attacked by protons. The linear relationship between $\Delta G(*NH_2 \rightarrow *NH_3)$ and the difference in total electrons (δ) on $*NH_2/*NH_3$ species demonstrates the great impact of B-to-adsorbate electron donation on determining the reaction energy at this elementary step. This influence is

opposite to the first hydrogenation step (Figure 3b) where electron donation is beneficial to high catalytic activity. These trends can explain our observation of the switch of PDS for MXene catalysts in different transition metal groups and suggest that a certain moderate degree of electron donation from the B center will be desirable to the overall catalytic activity.

Besides the consideration of catalytic activity, the difference between the limiting potentials for electrochemical NRR and the competing hydrogen evolution reaction (HER) is another metric for catalytic performance.[4,58] The limiting potential (U_L) is defined as the lowest negative potential at which all of the elementary steps are exergonic.[14] The catalytic activity for HER at the B center can be evaluated by the free energy profile shown in Figure 4a. The calculated free energy changes for HER are above those of NRR for all of the B-doped MXene catalysts. It is noted that Mo_2CO_2 and W_2CO_2 are located at the top right-hand corner of Figure 4b, indicating that they can combine excellent catalytic activity and high catalytic selectivity. Our results not only offer encouraging perspectives for further experimental examination of both materials as the potential catalyst candidates but also for the first time demonstrate the tenability of both catalytic activity and selectivity by a transition metal in the substrate, which can inspire and inform the design of novel single-boron catalysts for NRR.

In summary, we have conducted DFT calculations to evaluate the potential of single-boron catalysts with MXene substrates in electrochemical NRR and revealed the reaction mechanisms for B center catalysis. B-doped Mo_2CO_2 and W_2CO_2 are singled out as the most promising candidates with high catalytic activity and selectivity, on which the limiting potentials for NRR are only -0.20 and -0.24 V, respectively. Either the first or the last hydrogenation step is identified as the PDS, depending on the degree of B-to-adsorbate electron donation, which is governed by the interplay between transition-metal d orbitals and B p orbitals. A higher tendency of electron donation can enable efficient N_2 activation, whereas a lower tendency can grant the $*NH_2$ intermediate a radical nature that reduces the energy input for hydrogenation. In this regard, a certain moderate degree of electron donation, tunable by the transition metal in the catalyst substrates, would be desirable for NRR, which offers new insights toward the discovery of high-performance catalysts based on B centers.

◼ ASSOCIATED CONTENT

Ⓢ Supporting Information

The Supporting Information is available free of charge on the ACS Publications website at DOI: 10.1021/acs.jpclett.9b02741.

Computational details; binding energy of B in MXene; kinetic stability of B-doped MXenes; optimized geometry of the intermediates; charge variation of different moieties; and partial density of states (PDF)

◼ AUTHOR INFORMATION

Corresponding Author

*E-mail: panfeng@pkusz.edu.cn.

ORCID Ⓞ

Shunning Li: 0000-0002-5381-6025

Feng Pan: 0000-0002-8216-1339

Author Contributions

#S.Z. and S.L. contributed equally.

Notes

The authors declare no competing financial interest.

◼ ACKNOWLEDGMENTS

◼ REFERENCES

(1) Smil, V. Detonator of the population explosion. *Nature* **1999**, *400*, 415−415.

(2) Schlögl, R. Catalytic synthesis of ammonia−a "never-ending story"? *Angew. Chem., Int. Ed.* **2003**, *42*, 2004−2008.

(3) Bezdek, M. J.; Chirik, P. J. A fresh approach to ammonia synthesis. *Nature* **2019**, *568*, 464−466.

(4) Liu, H.; Wei, L.; Liu, F.; Pei, Z.; Shi, J.; Wang, Z.; He, D.; Chen, Y. Homogeneous, heterogeneous, and biological catalysts for electrochemical N₂ reduction toward NH₃ under ambient conditions. *ACS Catal.* **2019**, *9*, 5245−5267.

(5) Kandemir, T.; Schuster, M. E.; Senyshyn, A.; Behrens, M.; Schlögl, R. The haber-bosch process revisited: On the real structure and stability of "ammonia iron" under working conditions. *Angew. Chem., Int. Ed.* **2013**, *52*, 12723−12726.

(6) Ertl, G. Elementary steps in heterogeneous catalysis. *Angew. Chem., Int. Ed. Engl.* **1990**, *29*, 1219−1227.

(7) Gambarotta, S.; Scott, J. Multimetallic cooperative activation of N₂. *Angew. Chem., Int. Ed.* **2004**, *43*, 5298−5308.

(8) Jia, H. P.; Quadrelli, E. A. Mechanistic aspects of dinitrogen cleavage and hydrogenation to produce ammonia in catalysis and organometallic chemistry: Relevance of metal hydride bonds and dihydrogen. *Chem. Soc. Rev.* **2014**, *43*, 547−564.

(9) Anderson, J. S.; Rittle, J.; Peters, J. C. Catalytic conversion of nitrogen to ammonia by an iron model complex. *Nature* **2013**, *501*, 84−87.

(10) Hoffman, B. M.; Lukoyanov, D.; Yang, Z. Y.; Dean, D. R.; Seefeldt, L. C. Mechanism of nitrogen fixation by nitrogenase: The next stage. *Chem. Rev.* **2014**, *114*, 4041−62.

(11) van der Ham, C. J.; Koper, M. T.; Hetterscheid, D. G. Challenges in reduction of dinitrogen by proton and electron transfer. *Chem. Soc. Rev.* **2014**, *43*, 5183−91.

(12) Kyriakou, V.; Garagounis, I.; Vasileiou, E.; Vourros, A.; Stoukides, M. Progress in the electrochemical synthesis of ammonia. *Catal. Today* **2017**, *286*, 2−13.

(13) Guo, C.; Ran, J.; Vasileff, A.; Qiao, S.-Z. Rational design of electrocatalysts and photo(electro)catalysts for nitrogen reduction to ammonia (NH₃) under ambient conditions. *Energy Environ. Sci.* **2018**, *11*, 45−56.

(14) Cui, X.; Tang, C.; Zhang, Q. A review of electrocatalytic reduction of dinitrogen to ammonia under ambient conditions. *Adv. Energy. Mater.* **2018**, *8*, 1800369.

(15) Kitano, M.; Inoue, Y.; Yamazaki, Y.; Hayashi, F.; Kanbara, S.; Matsuishi, S.; Yokoyama, T.; Kim, S. W.; Hara, M.; Hosono, H. Ammonia synthesis using a stable electride as an electron donor and reversible hydrogen store. *Nat. Chem.* **2012**, *4*, 934−40.

(16) Kitano, M.; Kanbara, S.; Inoue, Y.; Kuganathan, N.; Sushko, P. V.; Yokoyama, T.; Hara, M.; Hosono, H. Electride support boosts nitrogen dissociation over ruthenium catalyst and shifts the bottleneck in ammonia synthesis. *Nat. Commun.* **2015**, *6*, 6731.

(17) Bao, D.; Zhang, Q.; Meng, F. L.; Zhong, H. X.; Shi, M. M.; Zhang, Y.; Yan, J. M.; Jiang, Q.; Zhang, X. B. Electrochemical reduction of N₂ under ambient conditions for artificial N₂ fixation and renewable energy storage using N₂ /NH₃ cycle. *Adv. Mater.* **2017**, *29*, 1604799.

(18) Li, S. J.; Bao, D.; Shi, M. M.; Wulan, B. R.; Yan, J. M.; Jiang, Q. Amorphizing of Au nanoparticles by CeOₓ-RGO hybrid support towards highly efficient electrocatalyst for N₂ reduction under ambient conditions. *Adv. Mater.* **2017**, *29*, 1700001.

(19) Guo, S.; Heck, K.; Kasiraju, S.; Qian, H.; Zhao, Z.; Grabow, L. C.; Miller, J. T.; Wong, M. S. Insights into nitrate reduction over indium-decorated palladium nanoparticle catalysts. *ACS Catal.* **2018**, *8*, 503−515.

(20) Nazemi, M.; Panikkanvalappil, S. R.; El-Sayed, M. A. Enhancing the rate of electrochemical nitrogen reduction reaction for ammonia synthesis under ambient conditions using hollow gold nanocages. *Nano Energy* **2018**, *49*, 316−323.

(21) Hirakawa, H.; Hashimoto, M.; Shiraishi, Y.; Hirai, T. Photocatalytic conversion of nitrogen to ammonia with water on surface oxygen vacancies of titanium dioxide. *J. Am. Chem. Soc.* **2017**, *139*, 10929−10936.

(22) Zhang, Y.; Qiu, W.; Ma, Y.; Luo, Y.; Tian, Z.; Cui, G.; Xie, F.; Chen, L.; Li, T.; Sun, X. High-performance electrohydrogenation of N₂ to NH₃ catalyzed by multishelled hollow Cr₂O₃ microspheres under ambient conditions. *ACS Catal.* **2018**, *8*, 8540−8544.

(23) Zhang, N.; Jalil, A.; Wu, D.; Chen, S.; Liu, Y.; Gao, C.; Ye, W.; Qi, Z.; Ju, H.; Wang, C.; Wu, X.; Song, L.; Zhu, J.; Xiong, Y. Refining defect states in W₁₈O₄₉ by mo doping: A strategy for tuning N₂ activation towards solar-driven nitrogen fixation. *J. Am. Chem. Soc.* **2018**, *140*, 9434−9443.

(24) Liu, Y.; Cheng, M.; He, Z.; Gu, B.; Xiao, C.; Zhou, T.; Guo, Z.; Liu, J.; He, H.; Ye, B.; Pan, B.; Xie, Y. Pothole-rich ultrathin WO₃ nanosheets triggering N≡N bond activation of nitrogen for direct nitrate photosynthesis. *Angew. Chem., Int. Ed.* **2019**, *58*, 731−735.

(25) Lv, C.; Yan, C.; Chen, G.; Ding, Y.; Sun, J.; Zhou, Y.; Yu, G. An amorphous noble-metal-free electrocatalyst that enables nitrogen fixation under ambient conditions. *Angew. Chem., Int. Ed.* **2018**, *57*, 6073−6076.

(26) Zhang, G.; Ji, Q.; Zhang, K.; Chen, Y.; Li, Z.; Liu, H.; Li, J.; Qu, J. Triggering surface oxygen vacancies on atomic layered molybdenum dioxide for a low energy consumption path toward nitrogen fixation. *Nano Energy* **2019**, *59*, 10−16.

(27) Abghoui, Y.; Garden, A. L.; Howalt, J. G.; Vegge, T.; Skúlason, E. Electroreduction of N₂ to ammonia at ambient conditions on mononitrides of Zr, Nb, Cr, and V: A DFT guide for experiments. *ACS Catal.* **2016**, *6*, 635−646.

(28) Abghoui, Y.; Garden, A. L.; Hlynsson, V. F.; Bjorgvinsdottir, S.; Olafsdottir, H.; Skulason, E. Enabling electrochemical reduction of nitrogen to ammonia at ambient conditions through rational catalyst design. *Phys. Chem. Chem. Phys.* **2015**, *17*, 4909−18.

(29) Abghoui, Y.; Skúlason, E. Onset potentials for different reaction mechanisms of nitrogen activation to ammonia on transition metal nitride electro-catalysts. *Catal. Today* **2017**, *286*, 69−77.

(30) Ren, X.; Cui, G.; Chen, L.; Xie, F.; Wei, Q.; Tian, Z.; Sun, X. Electrochemical N₂ fixation to NH₃ under ambient conditions: Mo₂N

nanorod as a highly efficient and selective catalyst. *Chem. Commun.* **2018**, *54*, 8474−8477.

(31) Azofra, L. M.; Li, N.; MacFarlane, D. R.; Sun, C. Promising prospects for 2d $d2-d4M_3C_2$ transition metal carbides (MXenes) in N_2 capture and conversion into ammonia. *Energy Environ. Sci.* **2016**, *9*, 2545−2549.

(32) Luo, Y.; Chen, G.-F.; Ding, L.; Chen, X.; Ding, L.-X.; Wang, H. Efficient electrocatalytic N_2 fixation with MXene under ambient conditions. *Joule* **2019**, *3*, 279−289.

(33) Rao, C. N. R.; Rao, G. R. Nature of nitrogen adsorbed on transition metal surfaces as revealed by electron spectroscopy and cognate techniques. *Surf. Sci. Rep.* **1991**, *13*, 223−263.

(34) Légaré, M.-A.; Bélanger-Chabot, G.; Dewhurst, R. D.; Welz, E.; Krummenacher, I.; Engels, B.; Braunschweig, H. Nitrogen fixation and reduction at boron. *Science* **2018**, *359*, 896−900.

(35) Hering-Junghans, C. Metal-free nitrogen fixation at boron. *Angew. Chem., Int. Ed.* **2018**, *57*, 6738−6740.

(36) Yu, X.; Han, P.; Wei, Z.; Huang, L.; Gu, Z.; Peng, S.; Ma, J.; Zheng, G. Boron-doped graphene for electrocatalytic N_2 reduction. *Joule* **2018**, *2*, 1610−1622.

(37) Ling, C.; Niu, X.; Li, Q.; Du, A.; Wang, J. Metal-free single atom catalyst for N_2 fixation driven by visible light. *J. Am. Chem. Soc.* **2018**, *140*, 14161−14168.

(38) Shi, L.; Li, Q.; Ling, C.; Zhang, Y.; Ouyang, Y.; Bai, X.; Wang, J. Metal-free electrocatalyst for reducing nitrogen to ammonia using a lewis acid pair. *J. Mater. Chem. A* **2019**, *7*, 4865−4871.

(39) Liu, C.; Li, Q.; Wu, C.; Zhang, J.; Jin, Y.; MacFarlane, D. R.; Sun, C. Single-boron catalysts for nitrogen reduction reaction. *J. Am. Chem. Soc.* **2019**, *141*, 2884−2888.

(40) Ji, S.; Wang, Z.; Zhao, J. A boron-interstitial doped C_2N layer as a metal-free electrocatalyst for N_2 fixation: A computational study. *J. Mater. Chem. A* **2019**, *7*, 2392−2399.

(41) Naguib, M.; Mashtalir, O.; Carle, J.; Presser, V.; Lu, J.; Hultman, L.; Gogotsi, Y.; Barsoum, M. W. Two-dimensional transition metal carbides. *ACS Nano* **2012**, *6*, 1322−1331.

(42) Anasori, B.; Lukatskaya, M. R.; Gogotsi, Y. 2D metal carbides and nitrides (MXenes) for energy storage. *Nat. Rev. Mater.* **2017**, *2*, 16098.

(43) Gao, G.; O'Mullane, A. P.; Du, A. 2D MXenes: A new family of promising catalysts for the hydrogen evolution reaction. *ACS Catal.* **2017**, *7*, 494−500.

(44) Li, N.; Chen, X.; Ong, W. J.; MacFarlane, D. R.; Zhao, X.; Cheetham, A. K.; Sun, C. Understanding of electrochemical mechanisms for CO_2 capture and conversion into hydrocarbon fuels in transition-metal carbides (MXenes). *ACS Nano* **2017**, *11*, 10825−10833.

(45) Handoko, A. D.; Khoo, K. H.; Tan, T. L.; Jin, H.; Seh, Z. W. Establishing new scaling relations on two-dimensional mxenes for CO_2 electroreduction. *J. Mater. Chem. A* **2018**, *6*, 21885−21890.

(46) Persson, I.; Halim, J.; Lind, H.; Hansen, T. W.; Wagner, J. B.; Naslund, L. A.; Darakchieva, V.; Palisaitis, J.; Rosen, J.; Persson, P. O. A. 2D transition metal carbides (MXenes) for carbon capture. *Adv. Mater.* **2019**, *31*, 1805472.

(47) Peng, J.; Chen, X.; Ong, W.-J.; Zhao, X.; Li, N. Surface and heterointerface engineering of 2d MXenes and their nanocomposites: Insights into electro- and photocatalysis. *Chem.* **2019**, *5*, 18−50.

(48) Li, L.; Wang, X.; Guo, H.; Yao, G.; Yu, H.; Tian, Z.; Li, B.; Chen, L. Theoretical screening of single transition metal atoms embedded in MXene defects as superior electrocatalyst of nitrogen reduction reaction. *Small Methods* **2019**, 1900337.

(49) Lukatskaya, M. R.; Mashtalir, O.; Ren, C. E.; Dall'Agnese, Y.; Rozier, P.; Taberna, P. L.; Naguib, M.; Simon, P.; Barsoum, M. W.; Gogotsi, Y. Cation intercalation and high volumetric capacitance of two-dimensional titanium carbide. *Science* **2013**, *341*, 1502−1505.

(50) Xie, Y.; Naguib, M.; Mochalin, V. N.; Barsoum, M. W.; Gogotsi, Y.; Yu, X. Q.; Nam, K. W.; Yang, X. Q.; Kolesnikov, A. I.; Kent, P. R. C. Role of surface structure on li-ion energy storage capacity of two-dimensional transition-metal carbides. *J. Am. Chem. Soc.* **2014**, *136*, 6385−6394.

(51) Honkala, K.; Hellman, A.; Remediakis, I. N.; Logadottir, A.; Carlsson, A.; Dahl, S.; Christensen, C. H.; Nørskov, J. K. Ammonia synthesis from first-principles calculations. *Science* **2005**, *307*, 555−558.

(52) Zhao, J.; Chen, Z. Single Mo atom supported on defective boron nitride monolayer as an efficient electrocatalyst for nitrogen fixation: A computational study. *J. Am. Chem. Soc.* **2017**, *139*, 12480−12487.

(53) Liu, J. C.; Ma, X. L.; Li, Y.; Wang, Y. G.; Xiao, H.; Li, J. Heterogeneous Fe_3 single-cluster catalyst for ammonia synthesis via an associative mechanism. *Nat. Commun.* **2018**, *9*, 1610.

(54) Liu, X.; Jiao, Y.; Zheng, Y.; Jaroniec, M.; Qiao, S. Z. Building up a picture of the electrocatalytic nitrogen reduction activity of transition metal single-atom catalysts. *J. Am. Chem. Soc.* **2019**, *141*, 9664−9672.

(55) Karlsson, L. H.; Birch, J.; Halim, J.; Barsoum, M. W.; Persson, P. O. Atomically resolved structural and chemical investigation of single MXene sheets. *Nano Lett.* **2015**, *15*, 4955−60.

(56) Liu, J.-C.; Tang, Y.; Wang, Y.-G.; Zhang, T.; Li, J. Theoretical understanding of the stability of single-atom catalysts. *Natl. Sci. Rev.* **2018**, *5*, 638−641.

(57) Anderson, J. S.; Cutsail, G. E., 3rd; Rittle, J.; Connor, B. A.; Gunderson, W. A.; Zhang, L.; Hoffman, B. M.; Peters, J. C. Characterization of an Fe≡N-NH$_2$ intermediate relevant to catalytic N_2 reduction to NH_3. *J. Am. Chem. Soc.* **2015**, *137*, 7803−7809.

(58) Skulason, E.; Bligaard, T.; Gudmundsdottir, S.; Studt, F.; Rossmeisl, J.; Abild-Pedersen, F.; Vegge, T.; Jonsson, H.; Nørskov, J. K. A theoretical evaluation of possible transition metal electrocatalysts for N_2 reduction. *Phys. Chem. Chem. Phys.* **2012**, *14*, 1235−1245.

(59) Comer, B. M.; Medford, A. J. Analysis of photocatalytic nitrogen fixation on rutile TiO_2(110). *ACS Sustainable Chem. Eng.* **2018**, *6*, 4648−4660.

(60) Khazaei, M.; Ranjbar, A.; Arai, M.; Sasaki, T.; Yunoki, S. Electronic properties and applications of MXenes: A theoretical review. *J. Mater. Chem. C* **2017**, *5*, 2488−2503.

(61) Clayborne, A.; Chun, H.-J.; Rankin, R. B.; Greeley, J. Elucidation of pathways for NO electroreduction on Pt(111) from first principles. *Angew. Chem., Int. Ed.* **2015**, *54*, 8255−8258.

(62) Chun, H.-J.; Apaja, V.; Clayborne, A.; Honkala, K.; Greeley, J. Atomistic insights into nitrogen-cycle electrochemistry: A combined DFT and kinetic Monte Carlo analysis of NO electrochemical reduction on Pt(100). *ACS Catal.* **2017**, *7*, 3869−3882.

(63) Zhao, J.; Zhang, L.; Xie, X.-Y.; Li, X.; Ma, Y.; Liu, Q.; Fang, W.-H.; Shi, X.; Cui, G.; Sun, X. Ti_3C_2Tx (T = F, OH) MXene nanosheets: Conductive 2d catalysts for ambient electrohydrogenation of N_2 to NH_3. *J. Mater. Chem. A* **2018**, *6*, 24031−24035.

(64) Ma, B.; Peng, Y.; Ma, D.; Deng, Z.; Lu, Z. Boron-doped InSe monolayer as a promising electrocatalyst for nitrogen reduction into ammonia at ambient conditions. *Appl. Surf. Sci.* **2019**, *495*, 143463.